LAWRENCE
LIVERMORE
NATIONAL
LABORATORY

LLNL-JRNL-414930

Detailed chemical kinetic mechanism for the oxidation of biodiesel fuels blend surrogate.

O. Herbinet, W. J. Pitz, C. K. Westbrook

July 21, 2009

Combustion and Flame

Disclaimer

Detailed chemical kinetic mechanism for the oxidation of biodiesel fuels blend surrogate.

Olivier Herbinet[1,2], William J. Pitz[1] and Charles K. Westbrook[1]
[1]Lawrence Livermore National Laboratory, California 94550, USA
[2]Département de Chimie Physique des Réactions, UMR 7630 CNRS, Nancy Université-ENSIC, 1 rue Grandville, 54000 Nancy, France

Full-length article

Corresponding author:
William J. Pitz
Lawrence Livermore National Laboratory
7000 East Avenue
Mail Stop L-372
Livermore, CA 94550
Tel: 925 422 7730
Fax: 925 424 4334
E-mail: pitz1@llnl.gov

Detailed chemical kinetic mechanism for the oxidation of biodiesel fuels blend surrogate.

Olivier Herbinet[1,2], William J. Pitz[1] and Charles K. Westbrook[1]
[1]Lawrence Livermore National Laboratory, California 94550, USA
[2]Département de Chimie Physique des Réactions, UMR 7630 CNRS, Nancy Université-ENSIC, 1 rue Grandville, 54000 Nancy, France

Abstract

Detailed chemical kinetic mechanisms were developed and used to study the oxidation of two large unsaturated esters: methyl-5-decenoate and methyl-9-decenoate. These models were built from a previous methyl decanoate mechanism and were compared with rapeseed oil methyl esters oxidation experiments in a jet stirred reactor. A comparative study of the reactivity of these three oxygenated compounds was performed and the differences in the distribution of the products of the reaction were highlighted showing the influence of the presence and the position of a double bond in the chain. Blend surrogates, containing methyl decanoate, methyl-5-decenoate, methyl-9-decenoate and n-alkanes, were tested against rapeseed oil methyl esters and methyl palmitate/n-decane experiments. These surrogate models are realistic kinetic tools allowing the study of the combustion of biodiesel fuels in diesel and homogeneous charge compression ignition engines.

Keywords

Methyl decanoate, methyl decenoate, surrogate, oxidation, biodiesel fuels, kinetic modeling, engine, low temperature

1. Introduction

Many studies have been performed to characterize the effects of the addition of oxygenated fuels to gasoline and diesel fuels on the emissions in engines. It has been observed that the use of oxygenated species leads to a decrease of the emissions of pollutants in general [1-3]. The combustion of biodiesel fuels in diesel engines allows lowering emissions of particulate matter, carbon monoxide and unburned hydrocarbons. A slight increase in the formation of nitrogen oxides is observed at some conditions. Biodiesel fuels have also the advantage of being alternative and renewable fuels contributing to the reduction of the dependence on crude oil importation and to environment preservation by lowering net emissions of carbon dioxide [4,5].

Biodiesel fuels are produced from mono-alkyl esters of long-chain fatty acids derived from vegetable oils and animal fats. These very large molecules are transformed into esters by reaction of trans-esterification with an alcohol. Methanol is commonly used but other alcohols, like ethanol, can also be employed. Most biodiesel fuels are made from rapeseed and soybean. Rapeseed and soybean derived biodiesels mainly contain the same five components: methyl palmitate ($C_{17}H_{34}O_2$), methyl stearate ($C_{19}H_{36}O_2$), methyl oleate ($C_{19}H_{34}O_2$), methyl linoleate ($C_{19}H_{32}O_2$) and methyl linolenate ($C_{19}H_{30}O_2$). The average compositions of soybean and rapeseed biodiesel fuels are displayed in Figure 1 [6]. These components have very similar structures (Figure 2): a methyl ester group attached to a large hydrocarbon chain. One difference is the length of the chain (16 atoms of carbon for methyl palmitate, 18 for the others) and the other difference in the number of double bonds in the chain: no double bond, one, two or three double bonds. According to Figure 1, most esters in soybean and rapeseed biodiesel fuels are unsaturated species. This justifies the development of detailed kinetic models for unsaturated methyl esters.

Figure 1

Figure 2

There have been many studies on the detailed chemical kinetics of methyl esters. Most of these studies have been on methyl butanoate ($C_5H_{10}O_2$). The first detailed

kinetic model for the oxidation of methyl butanoate was developed by Fischer et al. [7] in 2000. It was validated against limited available experimental pressure data in closed vessels [8]. More recently, this model has been used and revised by Metcalfe et al. [9] to reproduce experimental data obtained in a shock tube. Similarly Gaïl et al. [10] compared their experimental data obtained in a jet stirred reactor, a variable pressure flow reactor and an opposed-flow diffusion flame with a slightly modified mechanism based on the work of Fischer et al.. Dooley et al. studied methyl butanoate in shock tube and rapid compression machine. They made further modifications to the methyl butanoate mechanism [11] to reproduce their experimental data and also literature data from a stirred reactor, flow reactor, and opposed flow diffusion flame. Farooq et al. [12] measured the CO_2 yield from methyl butanoate pyrolysis in a shock tube and modified the methyl butanoate mechanism based on electronic structure calculations. These studies allowed clarifying the specific kinetic features due to the presence of the ester group.

The study of ignition delay times of methyl esters and biodiesel fuels droplets in microgravity showed that methyl butanoate is not a good surrogate for large methyl esters in biodiesel fuels [13]. Methyl butanoate is much less reactive than soybean biodiesel whereas larger species such as methyl decanoate and methyl dodecanoate have about the same reactivity as biodiesel. In their HCCI engine simulations of blends of soy-based biodiesel and ultra low sulfur diesel, Szybist et al. [14] speculated that the cetane number of methyl butanoate is too low to account for experimentally observed changes in burn duration and phasing when the biodiesel concentration was changed.

There have been relatively few studies on the chemical kinetics of large methyl esters. A model for the oxidation of a large ester, methyl decanoate (Figure 3), was developed by Herbinet et al. [15]. This model contains 8580 reactions and 3034 species. It was compared with rapeseed oil methyl esters experiments by Dagaut et al. [16]. The agreement between experimental and computed mole fractions is satisfactory and one feature of this model is its ability to reproduce the early formation of carbon dioxide due to the presence of the ester group. The model was also compared with n-decane ignition delay times in a shock tube. Computed ignition delay times were in very good agreement with n-decane experiments, except at the lowest temperature where methyl decanoate was a little bit less reactive than n-decane. These similarities in the reactivity have important implications in the

development of surrogate models: n-alkanes can be very good surrogates for the reactivity of methyl esters of similar size [15]. The methyl decanoate model was reduced and used to model extinction and ignition of laminar non-premixed flames containing methyl decanoate [17].

Methyl decanoate has no double bond whereas most esters in biodiesel fuels are unsaturated species. The presence of double bonds has an influence of the formation of unsaturated species, which are known to be precursors of soot. Their presence also affects the reactivity of the fuel mixture by restricting some low temperature reactions such as RO_2 isomerisations, allowing addition of radicals to the double bond, and leading to the formation of resonantly stabilized radicals.

Zhang et al. [18] studied saturated and unsaturated C_9 esters experimentally in a motored engine. They found that the presence of the double bond in the unsaturated C_9 ester reduced the reactivity of the fuel/air mixture compared to the saturated C_9 ester. They said that the lower reactivity in the low temperature regime can be explained by reduced amounts of 6 and 7-member transition states formed during the oxidation of the unsaturated methyl ester.

The present work intends to provide reliable detailed kinetic models for the oxidation of two esters having one double bond, methyl-5-decenoate and methyl-9-decenoate (Figure 3), in order to develop blend surrogate mechanisms more representative of biodiesel fuels. Methyl-9-decenoate was chosen because the double bond is at the same position as the one in methyl oleate and at same location as the first double bond in methyl linoleate and in methyl linolenate. Methyl-5-decenoate has been chosen to highlight the influence of the position of the double bond in the chain. These two models have been compared with rapeseed oil methyl esters experiments of Dagaut et al. [16]. To obtain improved surrogate mixture models to represent biodiesel fuels, models of binary and tertiary mixtures are compared to experimental measurements of binary component mixtures and of rapeseed oil methyl esters in a jet stirred reactor.

Figure 3

2. Description of the chemical kinetic mechanisms

The unsaturated and saturated methyl esters under investigation have similar molecular structures: they have a C_{10} hydrocarbon chain and a methyl ester group. The difference is the presence of a double bond in the hydrocarbon chains of methyl-5-decenoate and methyl-9-decenoate (Figure 3). Because of the similarities, some species generated by the reactions of unimolecular initiation and H-atom abstraction were already included in the previous methyl decanoate mechanism [15]. Thus the two sub-mechanisms for the oxidation of methyl-5-decenoate and methyl-9-decenoate were developed from the previous model for the oxidation of methyl decanoate by adding the chemistry specific to these unsaturated species.

The two sub mechanisms were developed by using the reaction classes from Curran et al. [19,20], but accommodations were required to take in account the specific chemistry due to the presence of the double bond and of the ester group. The reaction classes from Curran et al. were reviewed in the previous methyl decanoate paper [15] and the emphasis is given on the specific reactions due to the double bond in the present paper. The elementary steps and associated rate constants involved in detailed chemical kinetic models are also presented by Battin-Leclerc in a review about the low-temperature combustion of hydrocarbons [21].

2.1. High Temperature Part

The first steps considered in the consumption of the fuel were unimolecular initiation reactions. Their rate constants were specified in the reverse recombination direction, except for the scission of allylic C-C bonds which was considered in the forward direction. A rate constant of $1.0\times10^{16}\times\exp[-71000(\text{cal.mol}^{-1})/RT]$ s^{-1} was used for this last reaction [22]. Rate constants of other reactions of recombination are given in Table 1 for methyl-5-decenoate and in Table 2 for methyl-9-decenoate.

The fuel consumption reactions considered were reactions with small radicals. These reactions include both abstraction of H-atoms by radicals and addition of radicals to the C-C double bond. H-atom abstractions from the fuel by H, CH_3, C_2H_3, C_2H_5, O, O_2, OH, HO_2, CH_3O, and CH_3O_2 were considered. The distinction was made

between alkylic (primary, secondary), allylic (secondary), vinylic (secondary and tertiary) H-atoms, and the two H atoms bonded to the carbon atom adjacent to the carbonyl group (S_{co} H-atoms) (Figure 4). Like in the case of methyl decanoate, we used H atom abstraction rates from tertiary bonds in other molecules for S_{CO} H-atoms because they have C-H bond energies similar to those of tertiary C-H bonds. Kinetic parameters are those recommended by Curran et al. [23]. Reactions of addition of H-atoms, HO_2 and OH to the C-C double bond of the reactant were already included in the methyl decanoate mechanism [15].

Subsequently, we assembled reactions and estimated rate constants to consume the fuel radicals formed by the H-atom abstraction reactions. These reactions include radical decompositions and isomerizations. Reactions of decomposition of fuel radicals were written in the reverse direction (addition of radicals to double bonds) and kinetic parameters are from a review of Curran and from the methyl butanoate study [7]. As in the methyl decanoate model, the kinetic parameters for the reactions of addition of radicals to the oxygen of the C=O bond were updated from the study of the methyl radical addition to the C=O bond by Henry et al. [24].

Reactions of isomerizations through 3, 4, 5 and 6 member rings cyclic transition states were considered. Isomerizations involving the abstraction of vinylic H-atoms were not written because of their very high activation energies. An extra strain correction of 15 $kcal.mol^{-1}$ was added to the activation energy when the cyclic transition state had an embedded double bond [25].

The decomposition of alkenyl, allylic and vinylic radicals leads to the formation of unsaturated species. H-atom abstractions and retroene reactions were considered in a systematic way for these species. Only unimolecular decomposition by scission of allylic bonds was written for unsaturated primary products because this type of bond is weaker than an alkylic bond. Isomerizations of alkenyl, allylic and vinylic radicals were also written. The rate constants for decomposition of these radicals were specified through reverse additions. The kinetic parameters used for these reactions are the same than those presented in the reactant section above.

Figure 4

Table 1

Table 2

2.2 Low Temperature Part

The low temperature mechanism was built in the same way as in the case of methyl decanoate. Some accommodations were required to take in account the presence of double bonds and of vinylic and allylic H-atoms.

The first steps to consider in a low temperature mechanism are radical addition to O_2, for radicals deriving from the H-atom abstractions from the reactant. For these $R+O_2$ reactions, mesomeric forms need to be considered when R is allylic, to account for the two possible positions of the radical site. Figure 5 displays the two limit structures of the allylic radical obtained by H-atom abstraction from methyl-9-decenoate and the two corresponding reactions of addition to O_2. Reactions of addition to O_2 of radicals coming from the reactions of unimolecular initiation were considered in the case of methyl-9-decenaote (they were already included in the methyl decanoate mechanism), but not in the case of methyl-5-decenaote in order to substantially reduce the size of the model. This is justified by the fact that unimolecular initiations are not important in the low temperature region. The reactions of addition to O_2 involving radicals deriving from the addition of OH to methyl-9-decenaote and methyl-5-decenaote were written and the specific reactions of decomposition of the new radicals through the mechanism of Waddington were considered ($k=5.36\times10^{12}\times T^{-0.8}\times\exp[-10790(cal.mol^{-1})/RT\ s^{-1}]$) [26]. The mechanism of addition followed by a decomposition through a four member ring cyclic transition state proposed by Lodhi and Walker for allylic radicals was taken in account ($k=1.7\times10^{9}\times T\times\exp[-26228(cal.mol^{-1})/RT\ s^{-1}]$) [27].

Reactions of RO_2 isomerization to QOOH through 5, 6, 7 and 8 member cyclic transition states were considered. Rate constants used for these reactions depend on the number of atoms in the cyclic transition state and on the type of H-atoms which is shifted (Table 3). Subsequently, QOOH radicals react by reactions of decomposition to cyclic ethers, by reaction of decomposition to olefins + HO_2 and by reactions of addition to O_2 leading to OOQOOH radicals. As in the case of methyl decanoate, only the isomerizations of OOQOOH radicals to ketohydroperoxide + OH were written. Reaction of decomposition of ketohydroperoxide to OH and a radical by breaking of

the O-O bond were taken in account. At this time, we have not considered the direct reaction of RO_2 to olefin + HO_2 [28] since it was not included in the corresponding methyl decanoate mechanism. However, we will consider this reaction path in future work. Rate constants of all these reactions are identical to those used in the methyl decanoate mechanism [15].

Figure 5

Table 3

2.3. Thermodynamic properties

Standard enthalpies of formation ($\Delta H_f°$), entropies (S), and specific heats (C_p) of the species involved in the two models were calculated using the THERM program from Ritter and Bozzelli [29]. This program is based on the group and bond additivity methods and the statistical thermodynamics approach proposed by Benson [30]. The thermodynamic data are stored as two sets of 7 polynomial coefficients (Chemkin formalism).

As for methyl decanoate, we used the C–H bond dissociation energy (94.1 kcal mol^{-1}) proposed by El-Nahas et al. for C–H bonds in the alpha position of the carbonyl group of the ester function [31].

3. Results and discussion

The models of oxidation of methyl-9-decenaote and methyl-5-decenaote were compared to experimental data from the literature. The only unsaturated ester for which data exist in the literature are methyl crotonate ($C_5H_8O_2$) [32] and C_9 methyl esters [18]. Methyl crotonate is too small for a comparison with large esters such as methyl-9-decenaote and methyl-5-decenaote. The two models were also compared with rapeseed oil methyl esters oxidation experiments in a jet stirred reactor [16]. Rapeseed (or canola) oil methyl esters mainly contain unsaturated species, the most abundant being methyl oleate (Figure 1). This species has one double bond such as

methyl-9-decenaote and methyl-5-decenaote. It is also larger, but it assumed that these esters have similar reactivities as it is the case for saturated methyl esters larger than C_8 [33] and for n-alkanes larger than C_7 [34,35].

Reactivities of methyl decanoate, methyl-9-decenaote and methyl-5-decenaote were compared and the differences in the distributions of the products of the reaction were highlighted. The models were then combined together with a model for the oxidation of n-heptane to obtain new blend surrogate models more representative of biodiesel fuels.

3.1. Comparison of the models with experimental data

The detailed kinetic models for methyl-9-decenaote and methyl-5-decenaote were compared with rapeseed oil methyl esters oxidation experiments in a jet stirred reactor at 10 atm over the temperature range 800-1400K [16]. Experiments were carried out at a residence time of 1 s, a stoichiometric ratio of 0.5 and high dilution in helium. Species leaving the reactor were analyzed by gas chromatography (FID and TCD for their quantification; GC/MS for their identification). Mole fraction profiles were given for methane, hydrogen, carbon dioxide, carbon monoxide, oxygen and 1-alkenes from ethylene to 1-heptene. Dagaut et al. did not report any data about the formation of unsaturated methyl esters in this paper.

Inlet mole fractions used for the simulation were 8.18×10^{-4} for the ester (methyl-9-decenaote or methyl-5-decenaote), 2.44×10^{-2} for oxygen and 9.75×10^{-1} for nitrogen. In simulations, the ester inlet mole fraction was chosen to match the inlet carbon flux of methyl esters in the experiments. Figure 6 displays the comparison of the two models with experimental data. The general agreement between experimental and computed mole fraction is satisfactory for methyl-9-decenoate. The methyl-5-decenoate model well reproduces the mole fraction profiles of species such as CO_2 but significant deviations are observed for some other species such as ethylene, acetylene and carbon monoxide. Methyl-5-decenoate is less reactive than the two others fuels (methyl-9-decenoate and methyl decanoate) as computed mole fractions are smaller for CO and CO_2 and larger for O_2 in the case of methyl-5-decenoate.

It can be seen in Figure 6 that computed mole fractions of acetylene are much higher in the case of the two unsaturated esters than in the case of methyl decanoate.

This is in agreement with the observations of Sarathy et al. [32], who performed a comparative experimental study of the oxidation of methyl butanoate ($C_5H_{10}O_2$) and methyl crotonate ($C_5H_8O_2$) in a jet stirred reactor. Their study showed that higher level of unsaturated species (acetylene, propyne, benzene), which are precursors of soot, were detected in the case of methyl crotonate.

Figure 6

Figure 7 displays the flow consumption paths of the three esters at high temperature (900 K). These species are mainly consumed by H-atom abstractions by radicals such as OH, H and by the diradical O. In the case of methyl decanoate, the most important consumption path is the abstraction of the H-atoms attached to the carbon atom adjacent to the carbonyl group of the ester function. In the case of the two unsaturated esters, most important paths are abstractions of the allylic H-atoms and the abstraction of the H-atoms attached to the carbon atom adjacent to the carbonyl group of the ester function. Abstractions of vinylic H-atoms also occur at this temperature, but they only represent about 2% of the consumption of the reactant. Unsaturated esters are also consumed by reactions of addition of OH radicals and of H-atoms to the double bond. In the case of methyl-9-decenoate (ester with the double bond at the end of the chain), note that the reactions of addition to the secondary sp^2 carbon atom are more important than the reactions of additions to the tertiary sp^2 carbon atom. This is not observed in the case of methyl-5-decenoate because this species has only two tertiary sp^2 carbon atoms.

Figure 7

Figure 8 displays the flow consumption paths for the three esters at low temperature (650 K). The main routes of consumption are also the H-atom abstractions. At this temperature only H-atom abstractions by OH radicals play a role. For methyl decanoate, the most important path is the abstraction of the H-atoms attached to the carbon atom adjacent to the carbonyl group of the ester function. For the two unsaturated esters, the prevalent consumption routes are the abstractions of allylic H-atoms and then of the H-atoms attached to the carbon atom adjacent to the carbonyl group of the ester function. Note that the abstractions of vinylic H-atoms do

not occur at this temperature. Reactions of addition of OH to double bonds still occur at low temperature whereas the reaction of addition of an H-atom to the secondary carbon atom in methyl-9-decenoate is the only one which plays a role.

Figure 8

Figure 9 displays the reactive flow consumption paths of the radical md3j (a representative fuel radical of methyl decanoate whose structure is defined in Figure 9) at 650 and 900 K, and a residence time of 1 s. At both temperatures, this radical is obtained from methyl decanoate through the abstraction of a secondary H-atom by OH radicals (Figures 7 and 8). At low temperature, the radical md3j mainly reacts by addition with oxygen forming a ROO radical. This ROO radical isomerizes to three QOOH radicals, md3ooh2j, md3ooh5j and md3ooh6j. The radical "md3ooh2j" (the QOOH species on the left in Figure 9a) mainly leads to an ester with one double bond and a HO_2 radical by β-scission decomposition. It also reacts by second addition to O_2 to form a OOQOOH radicals which then decomposes to a ketohydroperoxide and an OH radical. The radical "md3ooh6j" (the QOOH species on the right in Figure 9a) mainly leads to the formation of a five member ring cyclic ether and an OH radical. It also reacts by second addition to O_2 to form a OOQOOH radicals which then decomposes to a ketohydroperoxide and an OH radical. The radical "md3ooh5j" (the QOOH radical in the middle in Figure 9a) reacts through three channels: 1) by a second addition to O_2 followed by a reaction of decomposition to ketohydroperoxide and OH; 2) by a reaction of decomposition to a four member ring cyclic ether and OH; 3) by a reaction of β-scission decomposition forming a 1-olefin and a keto-ester. The decomposition of ketohydroperoxide through the breaking of the O-O bond leads to low temperature chain branching and accelerates the oxidation rate of the fuel.

At high temperature (900 K, Figure 9b), the radical md3j mainly isomerizes forming other C_{11} alkyl-ester radicals and decomposes forming olefins and esters with one double bond at the end of the chain. The addition of O_2 still occurs at 900 K. The QOOH radicals deriving from this addition mainly react by β-scission decompositions and decompositions to cyclic ethers whereas the second addition to O_2 is not observed any more.

Figure 9

3.2. Comparison of the reactivity of the three methyl esters

The models of oxidation of methyl decanoate, methyl-9-decenaote and methyl-5-decenaote were used to compare their reactivity. Figure 10 displays the variation of ignition delay times with the temperature for the three species. Simulations were performed at a pressure of 1 atm and at stoichiometric conditions in air. The predictions show very close reactivities for the three esters with the main differences being visible in the negative coefficient temperature (NTC) region. Methyl-9-decenaote, with the double bond at the end of the alkyl chain, has the shortest ignition delay times and is the most reactive methyl ester component. The least reactive component is methyl-5-decenoate with a double bond in the middle of the carbon chain. Methyl decanoate (with no double bond) has a reactivity that lies in between the two other molecules. This comparison shows that the presence and the position of a double bond in the alkyl chain of a fuel component are very important in determining its reactivity. Vanhove et al. performed the experimental study of the influence of the position of the double bond in the reactivity of the three hexene isomers in a rapid compression machine [36]. They showed that the 1-hexene is the most reactive and that 3-hexene is the least reactive. Modeling studies showed that at low temperature, 1-hexene mainly leads to the formation of branching agents (ketohydroperoxides) whereas 2- and 3-hexenes mainly lead to the formation of di-olefins and low reactive HO_2 radicals [25,37]. Unfortunately, there are no shock tube or rapid compression machine experimental data in the literature showing the direct comparison of the reactivity of a n-alkane with the reactivities of the alkene isomers having the same number of carbon atoms.

Figure 10

According to the comparison between the different models (at jet-stirred reactor and shock tube conditions, Figure 6 and Figure 10), methyl-9-decenaote seems to be a better surrogate for unsaturated esters in real biodiesel fuels than methyl-5-decenaote. This is because the double bond in methyl-5-decenaote is close to the ester group

whereas the double bond in methyl-9-decenaote is at the same position as the one in methyl oleate and as the first one in methyl linoleate and methyl linolenate.

3.3. Surrogate blends

Models were assembled for blend surrogates in order to better represent the oxidation of real biodiesel fuels. A blend composed of methyl decanoate and n-heptane was already presented in a previous paper. It was compared to rapeseed oil methyl esters oxidation experiments in a jet stirred reactor [16] showing satisfactory agreement between experiment and modeling. This model is compared here to recent experiments of the oxidation of a blend of n-decane and methyl palmitate in a jet-stirred reactor over a wider range of temperatures (550-1100 K) including the NTC region [38]. Experiments were performed at a pressure of 106 kPa, a residence time of 1.5 s, and stoichiometric conditions with high dilution in helium. Fuel inlet mole fraction was set to 2×10^{-3}, oxygen mole fraction to 3.568×10^{-2} and helium mole fraction to 0.96232. The mole composition of the fuel mixture was 74% of n-decane and 26% of methyl palmitate. Simulations were performed at the same conditions of pressure, temperature and residence time. The mole fractions were adjusted in order to keep the carbon content and the ester group content constant and to remain at stoichiometric conditions. Inlet mole fraction of methyl decanoate was kept equal to 5.2×10^{-4}, n-heptane mole fraction was set to 2.56×10^{-3}, oxygen mole fraction to 3.622×10^{-2} and helium mole fraction to 0.9607. Figure 11 and Figure 12 display the comparison between the modeling and the experimental results. The agreement between computed and experimental data is satisfactorily for most species. Conversions of n-decane and methyl palmitate reproduce well the shape and position of the S-shape curve due to the negative coefficient of temperature, except that the two models seem to be too reactive in the range 800 – 900 K. The mole fraction profiles of species such as methane, acetylene, carbon oxides, methanol, methyl acrylate, 5-hexene methyl ester are rather well reproduced by the model. Methyl acrylate and 5-hexene methyl esters are characteristic intermediates from methyl ester oxidation. At high temperature, the overprediction of some species can be explained in terms of the overconversion of fuel from 800-900K mentioned earlier. However, mole fractions of ethylene and propyne are underpredicted for temperatures above

900K. The formation of acetaldehyde and propanal is too important at low temperature whereas propanone is underpredicted for all temperatures. 8-Nonene methyl ester is underpredicted because the alkyl chain in methyl decanoate in too short to account for the formation of a large methyl ester with one double bond at the end of the chain.

Figure 11

Figure 12

To more accurately simulate the oxidation of rapeseed oil methyl esters, a model for the oxidation of a ternary blend composed of methyl decanoate, methyl-9-decenoate and n-heptane was used to model the same oxidation experiments reported in Figure 6 [16]. Simulations were performed at the same conditions as in the experiments except that inlet mole fractions were adjusted to match the carbon and the ester group contents and to keep a stoichiometric ratio of 1. Inlet mole fractions are summarized in Table 4. Figure 13 displays the comparison between the blend surrogate model and the experiments. The agreement between computed and experimental mole fractions is globally satisfactory for most species. It can be seen that mole fractions of 1-hexene are underpredicted by the model. This is because the number of carbon atoms in n-heptane and in the chains of the esters is too short to account for the formation of large 1-olefins and methyl esters with a double bond at the end of the chain.

Table 4

Figure 13

3.4 Comparisons to motored engine experiments

Zhang et al. [18] have recently performed experiments on the oxidation of saturated and unsaturated C_9 methyl esters in a motored engine. For each C_9 methyl ester, they measured the intermediate species in the exhaust of the engine as the compression ratio was increased. At low compression ratios, little reaction of the

methyl ester was observed. As the compression ratio was increased, the amount of reaction increased until finally autoignition of the fuel/air mixture occurred and only carbon dioxide and water were observed in the exhaust products. To provide further confidence in the behavior of our models of C_{10} methyl esters, we used them to represent the C_9 methyl esters oxidation in these experiments.

We expect the reactivity of these large C_9 and C_{10} methyl esters to be similar because the reactivity of the large methyl ester is largely determined by the length of CH_2 chains contained in the hydrocarbon chain attached to the ester group. If there are a sufficient number of CH_2 groups in a series, RO_2 isomerizations will be very fast leading to low temperature reactivity in the engine. At least three CH_2 groups in a row are needed to allow 6-member transition states which have the fastest isomerization rates. If the CH_2 chain length is longer, more 6-member isomerizations are possible leading to more reactivity. One can compare the length of the CH_2 chains in the C_9 methyl esters examined in the engine study (Figure 14) with that of the C_{10} methyl esters in our model (Figure 3). We chose to compare the methyl-2-nonenoate with a five CH_2 group chain with the methyl-5-decenoate with two groups of three CH_2 chains. The three CH_2 chains give the sufficient length to allow RO_2 isomerizations with 6-member transition states.

Figure 14

We simulated the oxidation of the C_9 methyl esters in the engine using a single zone, homogeneous, engine model provided in the Senkin code of Chemkin 3 [39], a numerical model we successfully used in simulating similar experiments for methyl decanoate [15]. We accounted for heat transfer losses in the CFR engine by lowering the intake temperature until similar reactivity was achieved in the model as in the experiment. In the engine experiments, the intake temperature was maintained at 523K to fully vaporize the C_9 methyl esters. In the calculations, we lowered the intake temperature by 120K to match the overall reactivity seen in the experiments. The CFR engine has thick metal block which is cooled with water so that we expect significant heat losses from the fuel-air charge to the combustion chamber walls. The calculations matched other experimental conditions: engine speed of 600 rev/sec, fuel/air equivalence ratio of 0.25, intake pressure of 100 kPa, intake valve closing of

166° before top dead center (TDC), and exhaust valve opening of 153° after TDC. For the slider-crank formula in the engine model, the ratio of the connecting rod length to the crank-arm radius is 4.5.

Since this is a motored engine, it takes a number of engine cycles for the exhaust composition to reach steady-state. Since not all the contents of the combustion chamber are exhausted after each cycle, a residual fraction of species present at the end of the cycle needs to be added to the fresh fuel-air charge of the subsequent cycle (Figure 15). This residual fraction was assumed to be equal to 1/(compression ratio) which approximately accounts for volume of gas remaining at TDC in the engine and that is not exhausted after the end of the exhaust stroke. To achieve steady-state concentrations at the end of the engine cycle, about 9 cycles needed to be computed. For 9 cycles per compression ratio and the six compression ratios, 36 hrs of CPU time were used on a 3 GHz PC.

Figure 15

The comparison of the computed and measured results is shown in Figure 16. The CO_2 is quite well reproduced by the model and the CO is within a factor of 2 to 3. The profile shapes are well simulated by the model. For the hydrocarbon species, the CH_4 is well reproduced and the C_2H_4 and C_3H_6 are reproduced within a factor of 2-4. The profile shapes of CH_4 and C_2H_4 are well simulated by the model. The model C_3H_6 profile is shifted slightly to lower compression ratios compared to the experiments. As seen by the total carbon in the species measured by the experiments and computed in the model, the model is producing more of these species before high temperature ignition occurs at a compression ratio of 7.7. This discrepancy may be due to temperature inhomogeneities in the engine such as cooler regions near the walls and ring crevices with correspondingly different reactivities which are not treated by a single zone model. Probably a multizone model [40] is needed to addresses these inhomogeneities in the combustion chamber. After hot ignition, the total carbon in the model and experiment is nearly the same. The above model and experimental comparisons give some additional confidence that the model is performing in a reasonable way under engine conditions.

Figure 16

4. Conclusion

In this study, models for two unsaturated esters, methyl-5-decenoate and methyl-9-decenoate, were built using the reaction rules for alkenes. Some adaptations were required in order to adapt these rules to the case of esters. Both models were compared with rapeseed oil methyl esters experiments in a jet-stirred reactor. The general agreement between computed and experimental results was satisfactory for both models.

The comparison of ignition delay times computed with both mechanisms showed that methyl-9-decenoate is more reactive than methyl-5-decenoate, in particular in the NTC region. The lower reactivity of methyl-5-decenoate is due to more difficult isomerizations over the double bond. Thus methyl-9-decenoate, with the double bond at the end of the alkylic chain, seems to be a better surrogate than methyl-5-decenoate for unsaturated esters in real biodiesel fuels. It is the length of the continuously-saturated carbon chain in the reactant that determines its reactivity because it sets the range of possible RO_2 isomerizations.

Models of methyl decanoate, methyl-9-decenoate and n-heptane were combined in order to obtain a blend surrogate mechanism more representative of biodiesel fuels. This blend surrogate model was used to simulate rapeseed oil methyl esters experiments in a jet-stirred reactor. The model reproduced well the experimental mole fraction profiles of most species with good agreement. This model can also be used for the modeling of biodiesel fuels from various origins by adjusting the mole fractions of the three fuel components in the reactant mixture.

Finally, the methyl-2-decenoate was used as a surrogate fuel to simulate the partial oxidation of methyl-2-nonenoate in a motored engine. The CO, CO_2 and hydrocarbon species at the end of the engine cycle were similar in the measurements and simulations. These results give some confidence in the use of the chemical kinetic model under engine conditions.

Acknowledgment

This work performed under the auspices of the U.S. Department of Energy by Lawrence Livermore National Laboratory under Contract DE-AC52-07NA27344.

We wish to thank Mr. Yu Zhang, Dr. Yi Yang, and Prof. André L. Boehman for details on the engine experiments and for the experimental data in tabular form.

Supporting information

Thermodynamic databases

Chemical kinetic models

References

1. M.S. Graboski, R.L. McCormick, Prog. Energy Combust. Sci. 24 (1998) 125-164.

2. A.K. Agarwal, Prog. Energy Combust. Sci. 33 (2007) 233-271.

3. C.K. Westbrook, W.J. Pitz, H.J. Curran, J. Phys. Chem. A (110) (2006) 6912-6922.

4. K. Bozbas, Renew. Sust. Energ. Rev. 12 (2) (2008) 542-552.

5. A. Demirbas, Prog. Energy Combust. Sci. 31 (2005) 466-487.

6. J. Van Gerpen, B. Shanks, R. Pruszko, D. Clements, G. Knothe, Biodiesel Production Technology, National Renewable Energy Laboratory subcontractor report NREL/SR-510-36244, 2004.

7. E.M. Fisher, W.J. Pitz, H.J. Curran, C.K. Westbrook, Proc. Combust. Inst. 28 (2000) 1579-1586.

8. B.I. Parsons, C.J. Danby, J. Chem. Soc. (1956) 1795-1798.

9. W.K. Metcalfe, S. Dooley, H.J. Curran, J.M. Simmie, A.M. El-Nahas, M.V. Navarro, J. Phys. Chem. 111 (19) (2007) 4001-4014.

10. S. Gaïl, M.J. Thomson, S.M. Sarathy, S.A. Syed, P. Dagaut, P. Diévart, A.J. Marchese, F.L. Dryer, Proc. Combust. Inst. 31 (1) (2007) 305-311.

11. S. Dooley, H.J. Curran, J.M. Simmie, Combust. Flame 153 (1-2) (2008) 2-32.

12. A. Farooq, D.F. Davidson, R.K. Hanson, L.K. Huynh, A. Violi, Proc. Combust. Inst. 32 (1) (2009) 247-253.

13. T. Vaughn, M. Hammill, M. Harris, A.J. Marchese, Ignition Delay of Bio-Ester Fuel Droplets, SAE Technical Paper Series, 2006-01-3302.

14. J.P. Szybist, J. McFarlane, B.G. Bunting, "Comparison of Simulated and Experimental Combustion of Biodiesel Blends in a Single Cylinder Diesel HCCI Engine", Society of Automotive Engineers Paper No. 2007-01-4010, 2007.

15. O. Herbinet, W.J. Pitz, C.K. Westbrook, Combust. Flame 154 (2008) 507-528.

16. P. Dagaut, S. Gaïl, M. Sahasrabudhe, Proc. Combust. Inst. 31 (2) (2007) 2955-2961.

17. K. Seshadri, T. Lu, O. Herbinet, S. Humer, U. Niemann, W.J. Pitz, C.K. Law, Proc. Combust. Inst. 32 (2009) 1067–1074.

18. Y. Zhang, Y. Yang, A.L. Boehman, Combust. Flame 156 (2009) 1202–1213.

19. H.J. Curran, P. Gaffuri, W.J. Pitz, C.K. Westbrook, Combust. Flame 129 (2002) 253-280.

20. H.J. Curran, P. Gaffuri, W.J. Pitz, C.K. Westbrook, Combust. Flame 114 (1998) 149-177.

21. F. Battin-Leclerc, Prog. Energy Combust. Sci. 34 (2008) 440–498.

22. T.C. Brown, K.D. King, T.T. Nguyen, J. Phys. Chem. 90 (3) (1986) 419-424.

23. H.J. Curran, Int. J. Chem. Kinet. 38 (4) (2006) 250-275.

24. D.J. Henry, M.L. Coote, R. Gomez-Balderas, L. Radom, J. Am. Chem. Soc. 126 (6) (2004) 1732-1740.

25. R. Bounaceur, V. Warth, B. Sirjean, P.A. Glaude, R. Fournet, F. Battin-Leclerc, Proc. Combust. Inst. 32 (2009) 387 394.

26. M.S. Stark, R.W. Waddington, Int. J. Chem. Kinet. 27 (1995) 123–151.

27. Z.H. Lodhi, R.W. Walker, J. Chem. Soc. Faraday T. 87 (15) (1991) 2361-2365.

28. C.A. Taatjes, J. Phys. Chem. A 110(13) (2006) 4299-4312.

29. E.R. Ritter, J. W. Bozzelli, Int. J. Chem. Kinet. 23 (1991) 767-778.

30. S.W. Benson, Thermochemical Kinetics, John Wiley and Sons Inc., New York, 1976.

31. A.M. El-Nahas, M.V. Navarro, J.M. Simmie, J.W. Bozzelli, H.J. Curran, S. Dooley, W. Metcalfe, J. Phys. Chem. A 111 (19) (2007) 3727-3739.

32. S.M. Sarathy, S. Gaïl, S.A. Syed, M.J. Thomson, P. Dagaut, Proc. Combust. Inst. 31 (1) (2007) 1015-1022.

33. J. Biet, V. Warth, O. Herbinet, P.A. Glaude, F. Battin-Leclerc, Proceedings of the European Combustion Meeting 2009, Vienna, Austria, April 14-17, 2009.

34. J. Biet, M.H. Hakka, V. Warth, P.A. Glaude, F. Battin-Leclerc, Energ. Fuel, 22 (4) (2008) 2258-2269.

35. C.K. Westbrook, W.J. Pitz, O. Herbinet, H.J. Curran, E.J. Silke, Combust. Flame 156 (2009) 181–199.

36. G. Vanhove, M. Ribaucour, R. Minetti, Proc. Combust. Inst. 30 (2005) 1065-1072.

37. M. Mehl, G. Vanhove, W.J. Pitz, E. Ranzi, Combust. Flame 155 (2008) 756-772.

38. M.H. Hakka, P.A. Glaude, O. Herbinet, F. Battin-Leclerc, Combust Flame (2009), doi:10.1016/j.combustflame.2009.06.003.

39. R. J. Kee, F. M. Rupley, J. A. Miller, M. E. Coltrin, J. F. Grcar, E. Meeks, H. K. Moffat, A. E. Lutz, G. Dixon-Lewis, M. D. Smooke, J. Warnatz, G. H. Evans, R. S. Larson, R. E. Mitchell, L. R. Petzold, W. C. Reynolds, M. Caracotsios, W. E. Stewart, P. Glarborg, C. Wang and O. Adigun, "CHEMKIN Collection, Release 3," Reaction Design, Inc., San Diego, CA, 2000.

40. R. P. Hessel, D. E. Foster, S. M. Aceves, M. L. Davisson, F. Espinosa-Loza, D. L. Flowers, W. J. Pitz, J. E. Dec, M. Sjöberg and A. Babajimopoulos, "Modeling Iso-octane HCCI using CFD with Multi-Zone Detailed Chemistry; Comparison to Detailed Speciation Data over a Range of Lean Equivalence Ratios," 2008 SAE World Congress, SAE 2008-01-0047, Detroit, MI, 2008.

Table 1: Unimolecular initiations for methyl-5-decenoate

Reaction of recombination	Rate constant ($cm^3.mol^{-1}.s^{-1}$)
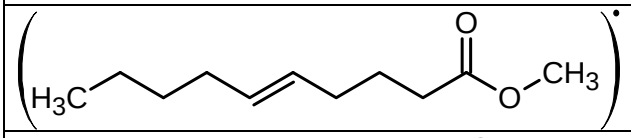	1.0×10^{14}
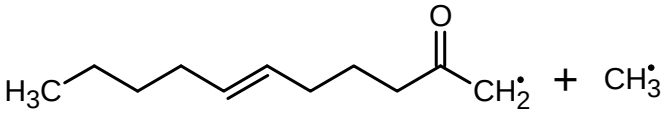	3.0×10^{13}
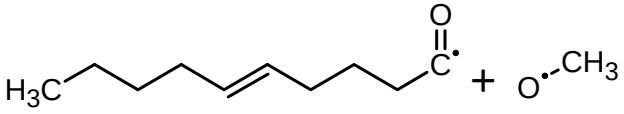	3.0×10^{13}
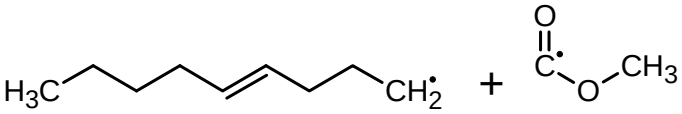	1.8×10^{13}
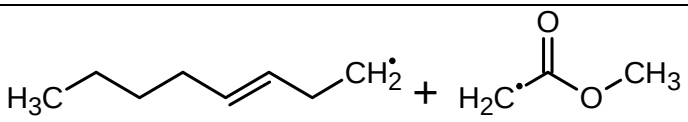	8.0×10^{12}
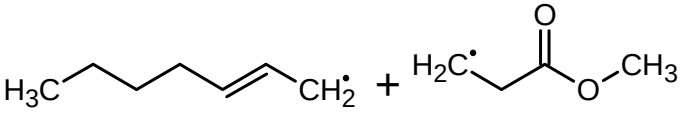	considered through the reverse direction (see text)
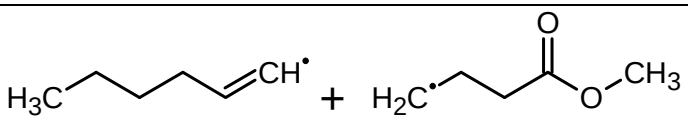	8.0×10^{12}
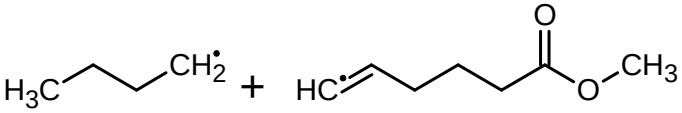	8.0×10^{12}
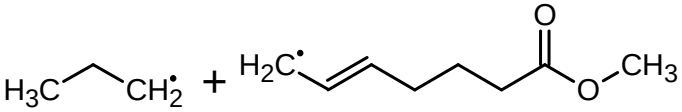	considered through the reverse direction (see text)
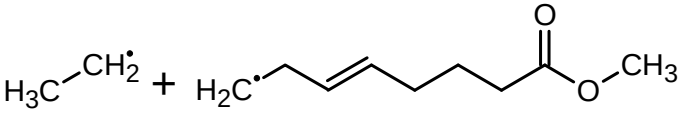	8.0×10^{12}
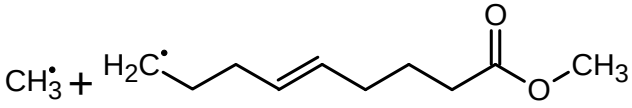	3.0×10^{13}

Table 2: Unimolecular initiations for methyl-9-decenoate

Reaction of recombination	Rate constant ($cm^3.mol^{-1}.s^{-1}$)
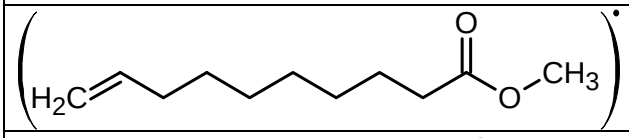	1.0×10^{14}
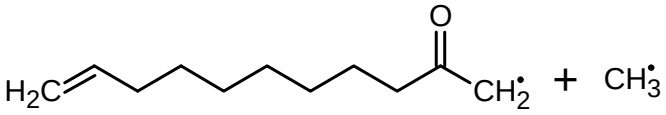	3.0×10^{13}
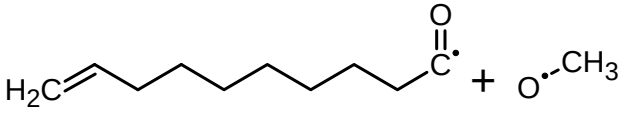	3.0×10^{13}
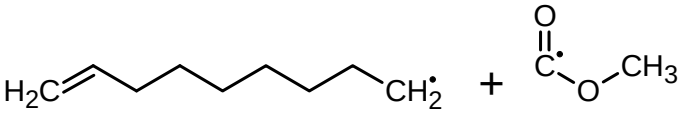	1.8×10^{13}
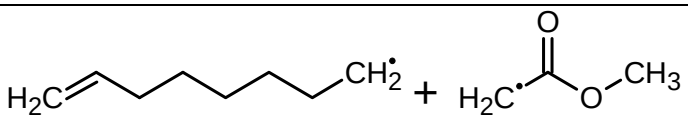	8.0×10^{12}
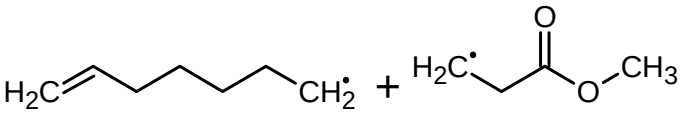	8.0×10^{12}
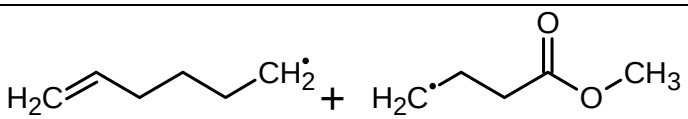	8.0×10^{12}
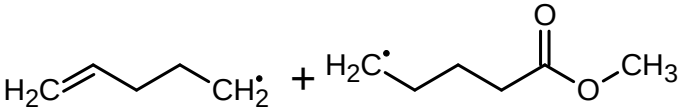	8.0×10^{12}
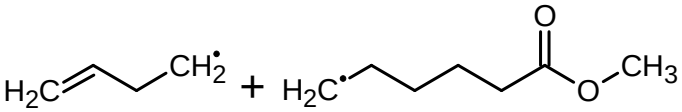	8.0×10^{12}
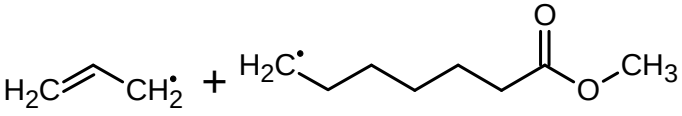	considered through the reverse direction (see text)
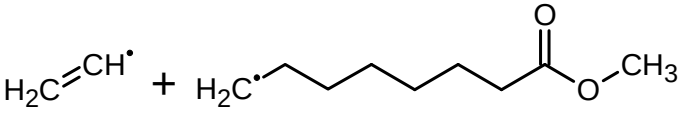	8.0×10^{12}

Table 3: Rate constants of the reactions of isomerization of RO_2 to QOOH ($k=A\times T^b\times\exp(E_a/RT)$) [Units: kcal, cm3, mol]

Number of atoms in the ring of the cyclic transition state	Type of H shifted (see Figure 4)	A	b	E_a
5 atoms ring	P	1.00×10^{11}	0.0	29.40
	S	1.00×10^{11}	0.0	26.85
	S_{CO}[1]	1.00×10^{11}	0.0	24.10
	AS	1.00×10^{11}	0.0	22.35
	VS	1.00×10^{11}	0.0	30.70
	VT	1.00×10^{11}	0.0	28.65
6 atoms ring	P	1.25×10^{10}	0.0	24.40
	S	1.25×10^{10}	0.0	20.85
	S_{CO}[1]	1.25×10^{10}	0.0	19.10
	AS	1.25×10^{10}	0.0	16.35
	VS	1.25×10^{10}	0.0	25.70
	VT	1.25×10^{10}	0.0	22.65
7 atoms ring	P	1.56×10^{09}	0.0	22.35
	S	1.56×10^{09}	0.0	19.05
	S_{CO}[1]	1.56×10^{09}	0.0	17.05
	AS	1.56×10^{09}	0.0	14.55
	VS	1.56×10^{09}	0.0	23.65
	VT	1.56×10^{09}	0.0	20.85
8 atoms ring	P	1.95×10^{08}	0.0	25.55
	S	1.95×10^{08}	0.0	22.05
	S_{CO}[1]	1.95×10^{08}	0.0	20.05
	AS	1.95×10^{08}	0.0	17.55
	VS	1.95×10^{08}	0.0	26.85
	VT	1.95×10^{08}	0.0	23.85

[1] it is assumed that this type of H atom react in a similar way than a tertiary H atom because the bond energies of the C-H bonds are very close.

Table 4: Inlet composition of the reacting mixture used for the methyl decanoate/ methyl-9-decenoate/n-heptane surrogate simulation in a jet-stirred reactor.

	Mole fraction
Methyl decanoate	2.50×10-4
Methyl-9-decenoate	2.50×10-4
n-Heptane	5.00×10-4
Oxygen	2.47×10-2
Helium	9.74×10-1

Figure captions:

Figure 1: Average composition of soybean and rapeseed biodiesels [6]. C16:0 = methyl palmitate, C18:0 = methyl stearate, C18:1 = methyl oleate, C18:2 = methyl linoleate and C18:3 = methyl linolenate.
Figure 2: Structures of the main components in soybean and rapeseed biodiesels.
Figure 3: Structures of methyl decanoate, methyl-5-decenoate and methyl-9-decenaote.
Figure 4: Different types of H-atoms considered for the H-atom abstractions. P = primary alkylic, S = secondary alkylic, SCO = secondary alkylic adjacent to the carbonyl group, AS = secondary allylic, VS = secondary vinylic and VT = tertiary vinylic H-atom.
Figure 5: The two possible reactions of addition to O2 of the allylic radical obtained by H-atom abstraction from methyl-9-decenoate.
Figure 6: Comparison of the three models with jet-stirred reactor experimental data (experimental data, – – – methyl decanoate model, —— methyl-9-decenoate model, •••••• methyl-5-decenoate model).
Figure 7: Flow decomposition paths of esters in the high temperature region (900 K). a) methyl decanoate; b) methyl-5-decenoate; c) methyl-9-decenoate.
Figure 8: Flow decomposition paths of esters in the low temperature region (650 K). a) methyl decanoate; b) methyl-5-decenoate; c) methyl-9-decenoate.
Figure 9: Flow decomposition paths of the radical md3j (formed from methyl decanoate) a) in the low temperature region (650 K) and b) in the high temperature region (900 K).
Figure 10: Comparison of the reactivity of methyl esters under shock tube conditions (stoichiometric fuel/air mixtures at 1 atm).
Figure 11: Comparison of the n-heptane/methyl decanoate model (——) with n decane/methyl palmitate jet-stirred experiments ( ) [37]. Conversion of reactants and mole fraction profiles of hydrocarbon products.
Figure 12: Comparison of the n-heptane/methyl decanoate model (——) with n decane/methyl palmitate jet-stirred experiments ( ) [37]. Mole fraction profiles of oxygenated compounds.
Figure 13: Comparison of the n-heptane/methyl decanoate/methyl-9-decenoate model (——) with rapeseed oil methyl esters jet-stirred experiments ( ) [16].
Figure 14: Structures of C9 methyl esters investigated in a motored engine study [18].
Figure 15: Gases in the residual part of the cylinder were taking in account by considering consecutive cycles. (ICE=internal combustion engine)
Figure 16: Comparison of predicted and measured [18] species exhausted from the motored engine. (Fuel: methyl-5-decenoate (model), methyl 2-nonenoate (experiments). Equivalence ratio of 0.25 and 600 rev/min.

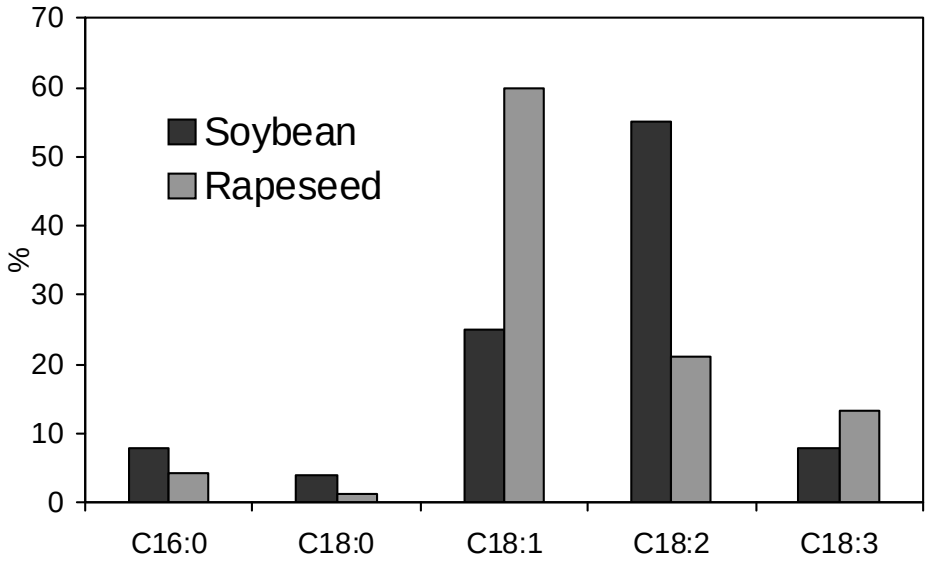

Figure 1: Average composition of soybean and rapeseed biodiesels [6]. C16:0 = methyl palmitate, C18:0 = methyl stearate, C18:1 = methyl oleate, C18:2 = methyl linoleate and C18:3 = methyl linolenate.

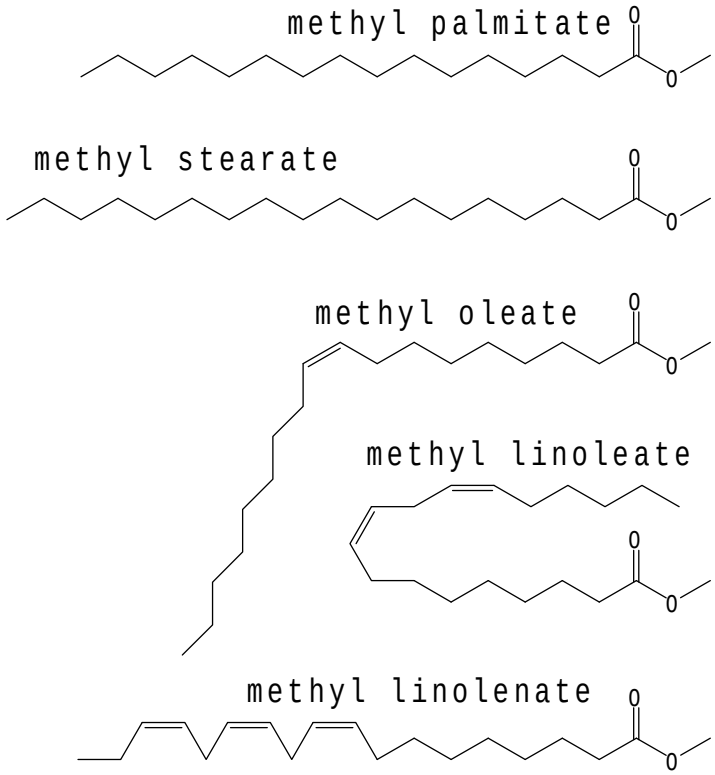

Figure 2: Structures of the main components in soybean and rapeseed biodiesels.

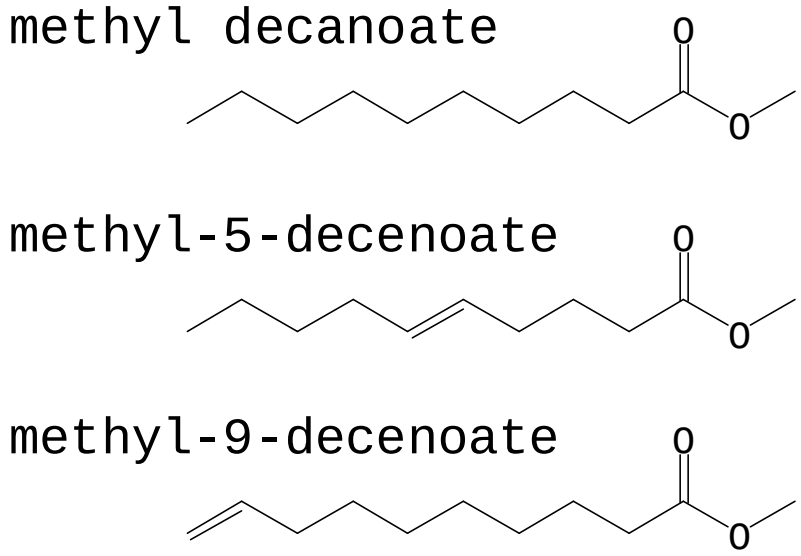

Figure 3: Structures of methyl decanoate, methyl-5-decenoate and methyl-9-decenaote.

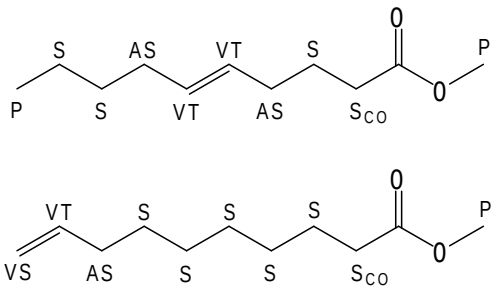

Figure 4: Different types of H-atoms considered for the H-atom abstractions. P = primary alkylic, S = secondary alkylic, S_{CO} = secondary alkylic adjacent to the carbonyl group, AS = secondary allylic, VS = secondary vinylic and VT = tertiary vinylic H-atom.

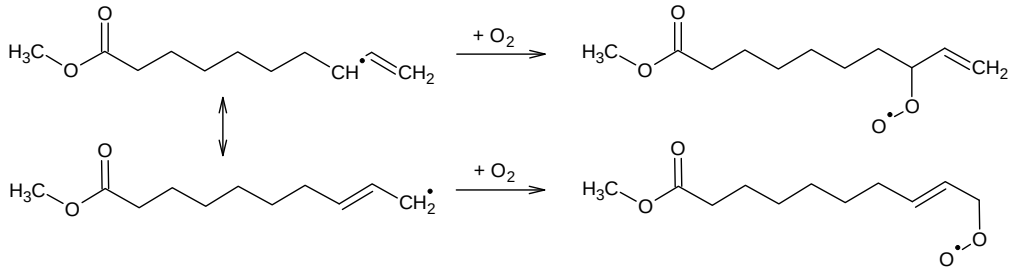

Figure 5: The two possible reactions of addition to O_2 of the allylic radical obtained by H-atom abstraction from methyl-9-decenoate.

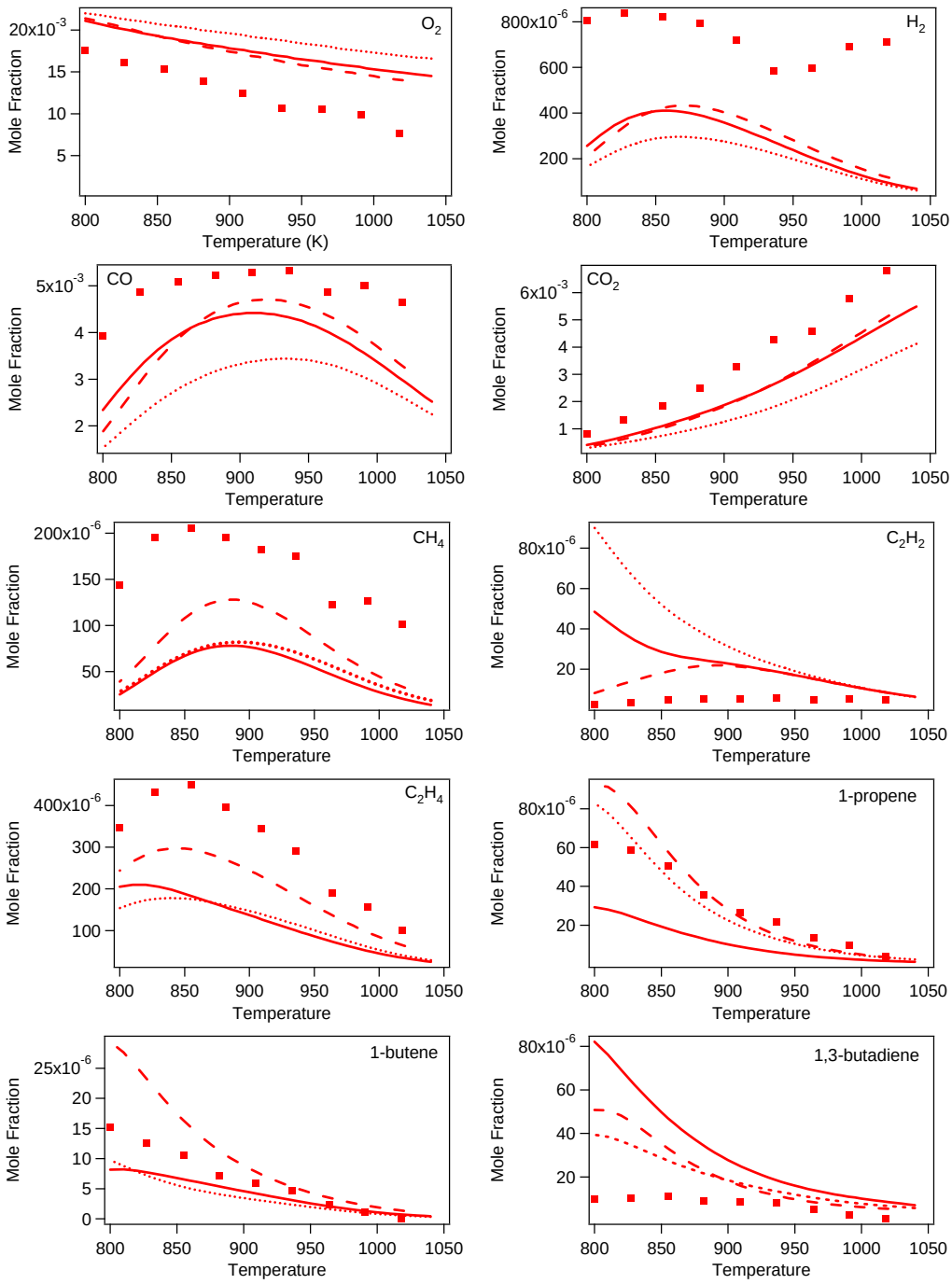

Figure 6: Comparison of the three models with jet-stirred reactor experimental data (▪ experimental data, – – – methyl decanoate model, —— methyl-9-decenoate model, •••••• methyl-5-decenoate model).

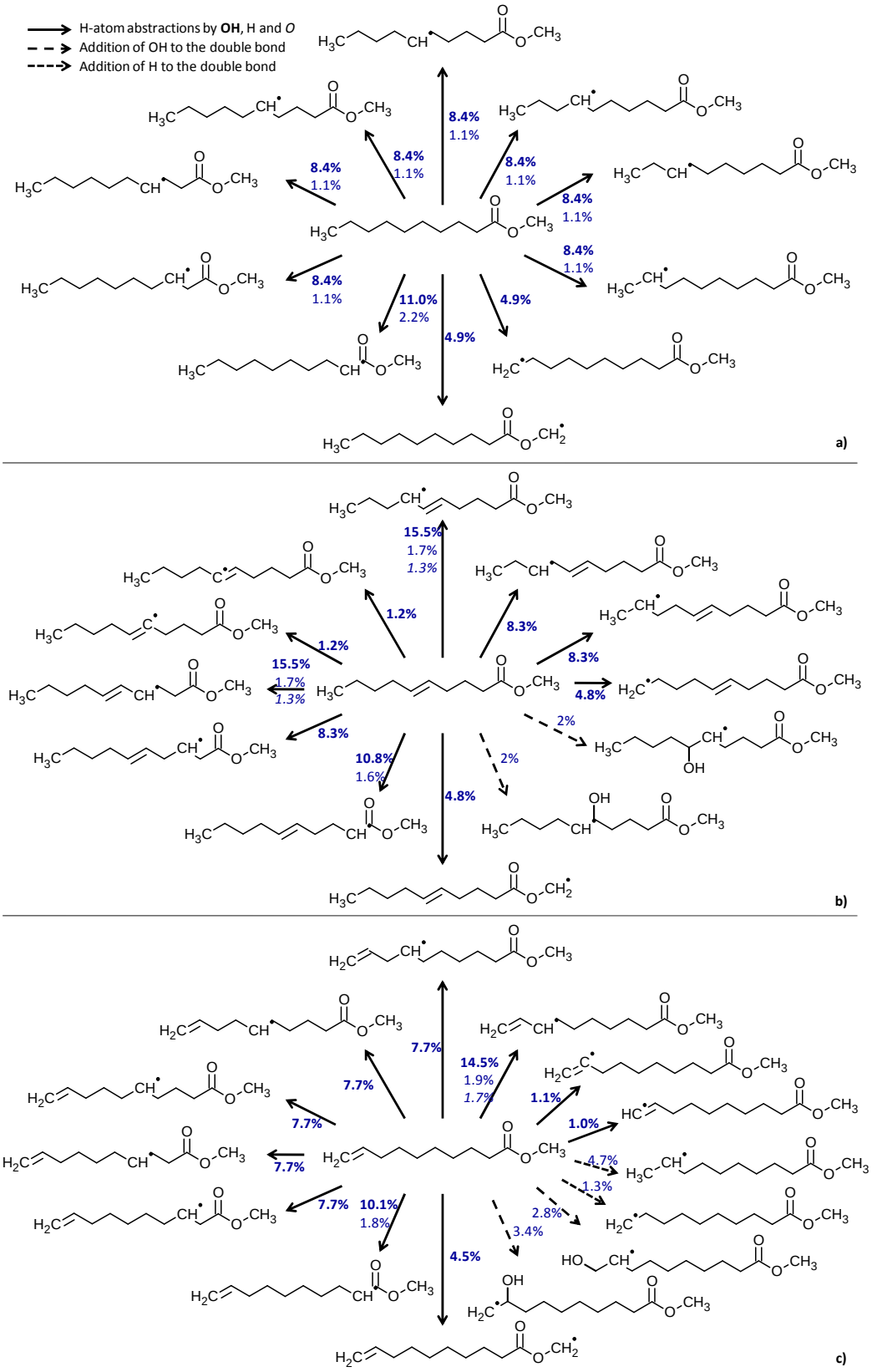

Figure 7: Flow decomposition paths of esters in the high temperature region (900 K). a) methyl decanoate; b) methyl-5-decenoate; c) methyl-9-decenoate.

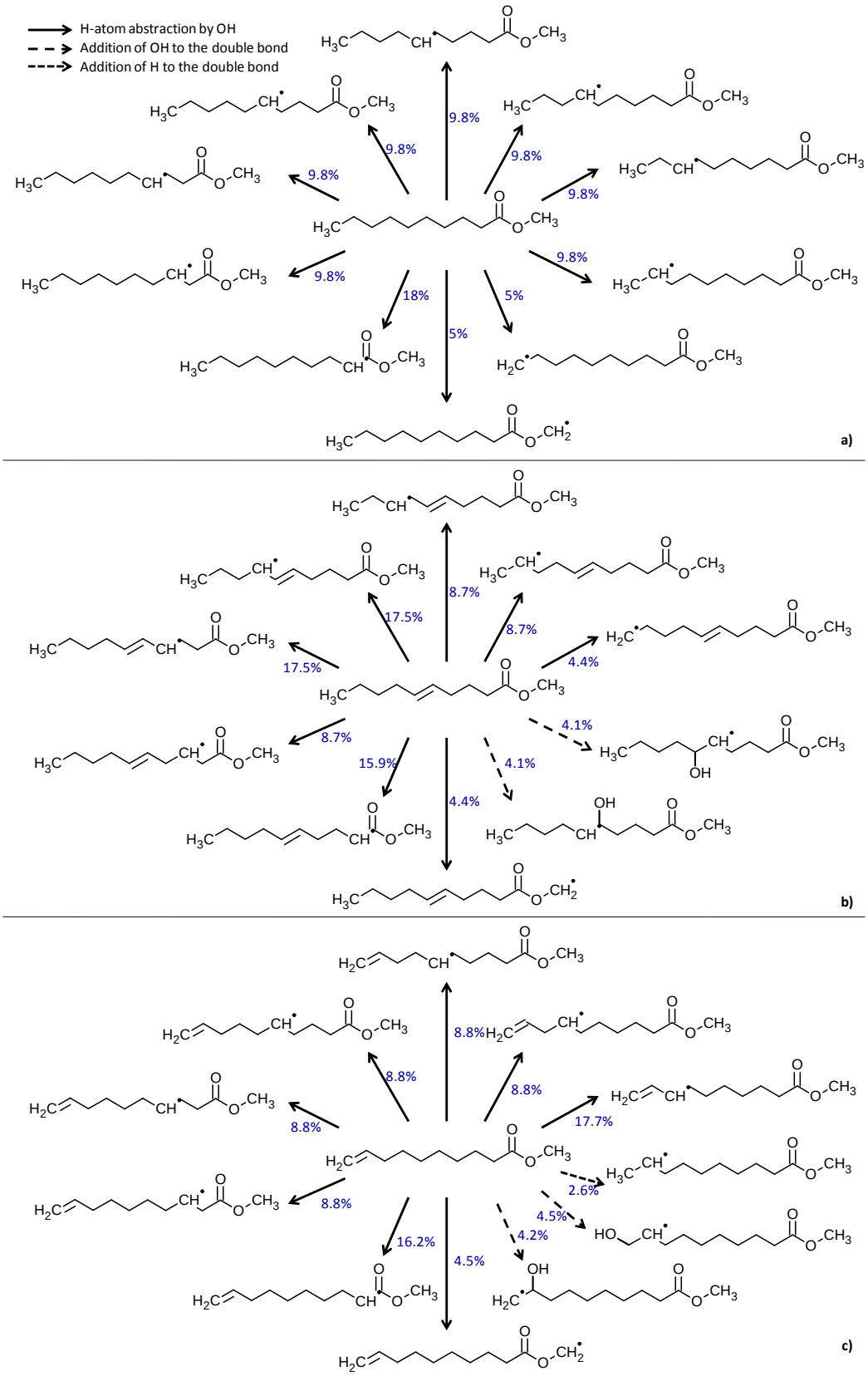

Figure 8: Flow decomposition paths of esters in the low temperature region (650 K). a) methyl decanoate; b) methyl-5-decenoate; c) methyl-9-decenoate.

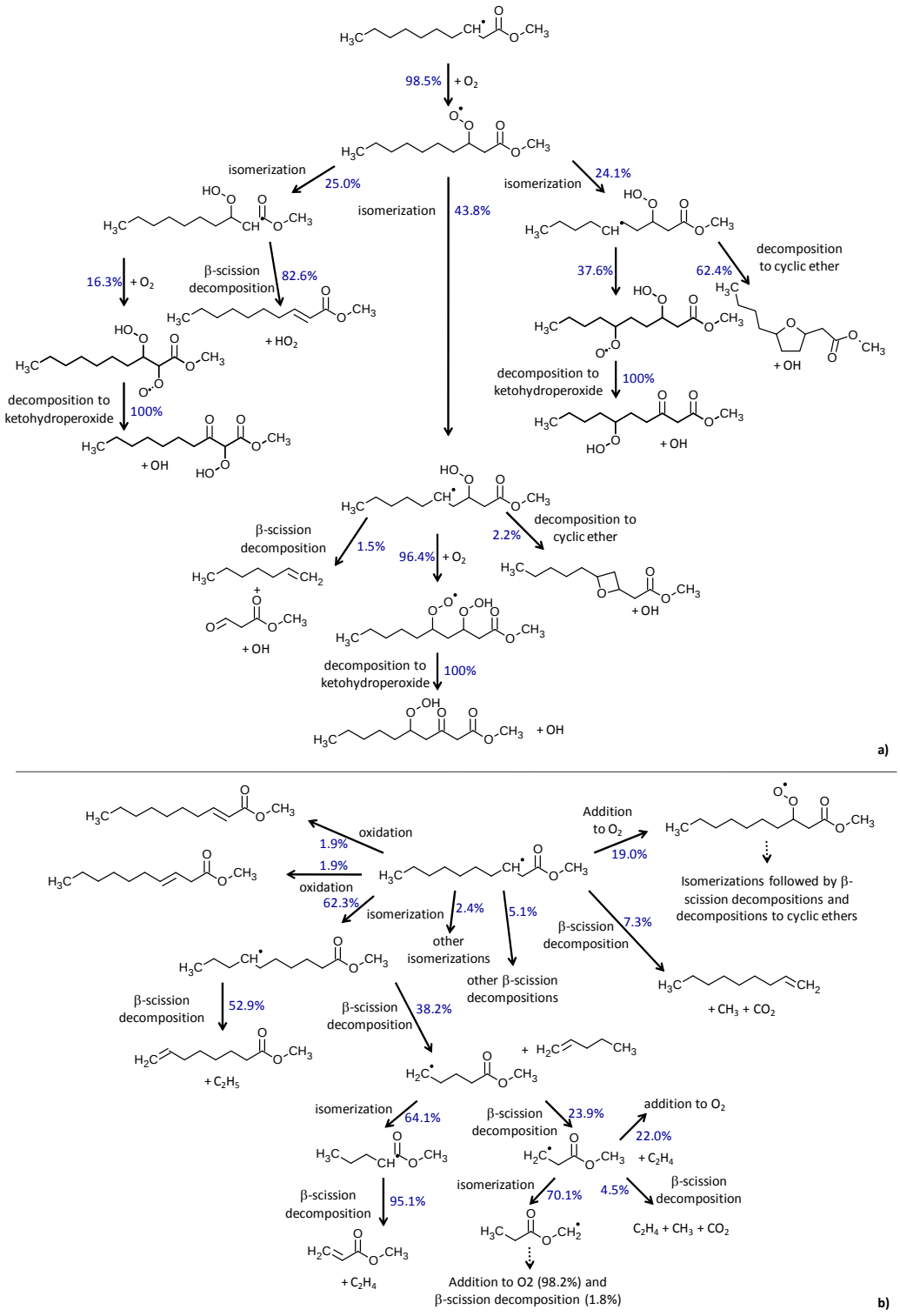

Figure 9: Flow decomposition paths of the radical md3j (formed from methyl decanoate) a) in the low temperature region (650 K) and b) in the high temperature region (900 K).

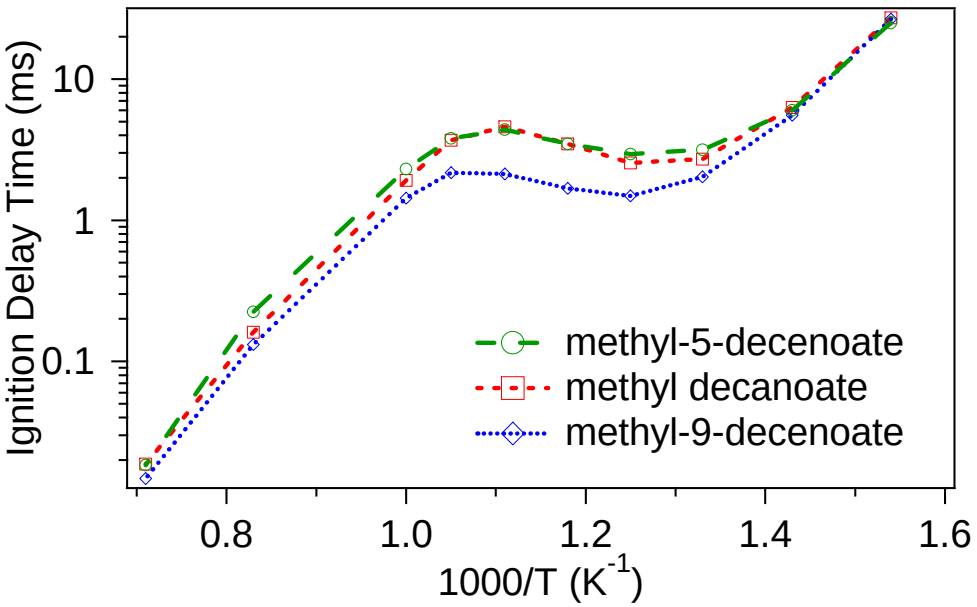

Figure 10: Comparison of the reactivity of methyl esters under shock tube conditions (stoichiometric fuel/air mixtures at 1 atm).

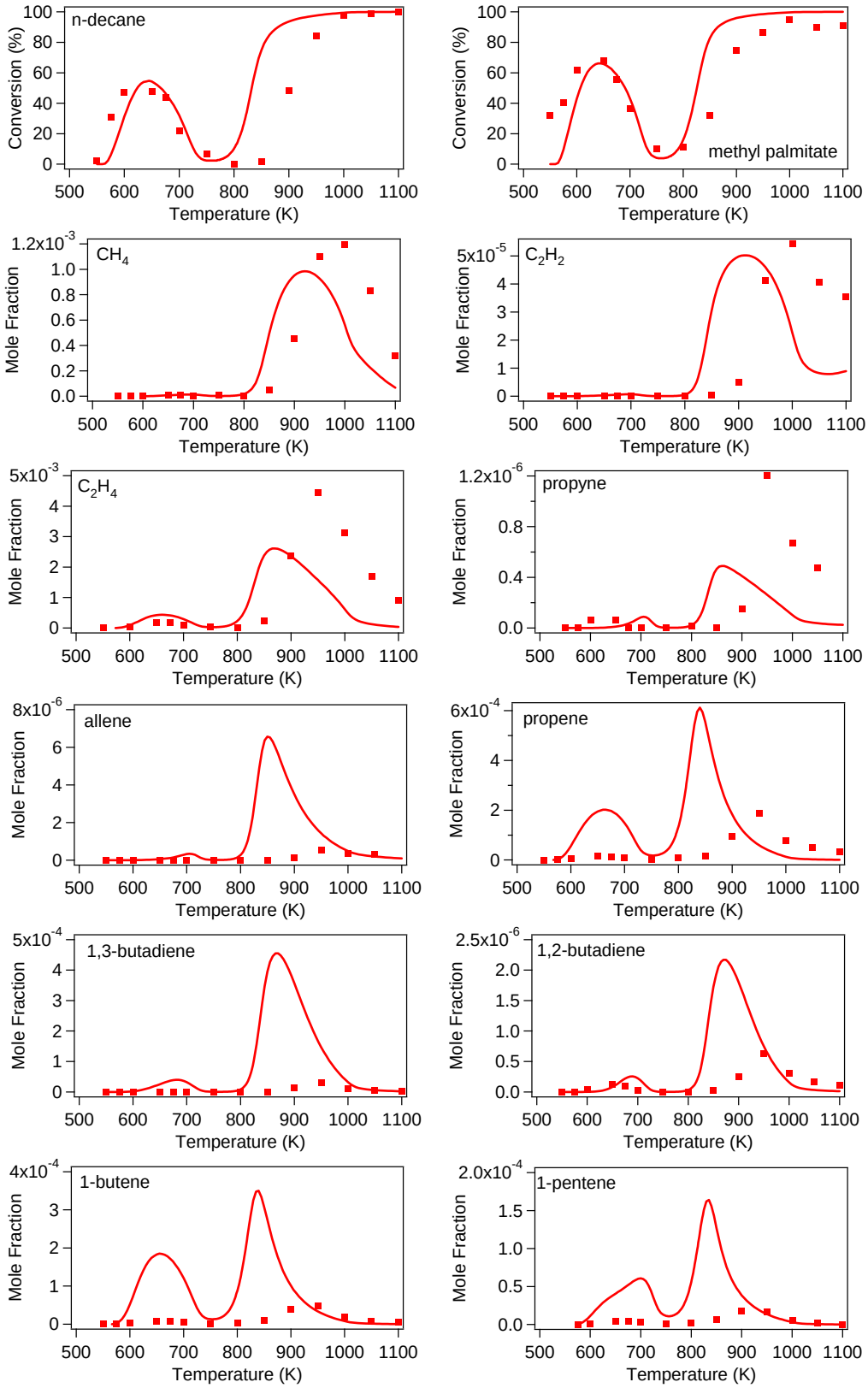

Figure 11: Comparison of the n-heptane/methyl decanoate model (——) with n-decane/methyl palmitate jet-stirred experiments (■) [38]. Conversion of reactants and mole fraction profiles of hydrocarbon products.

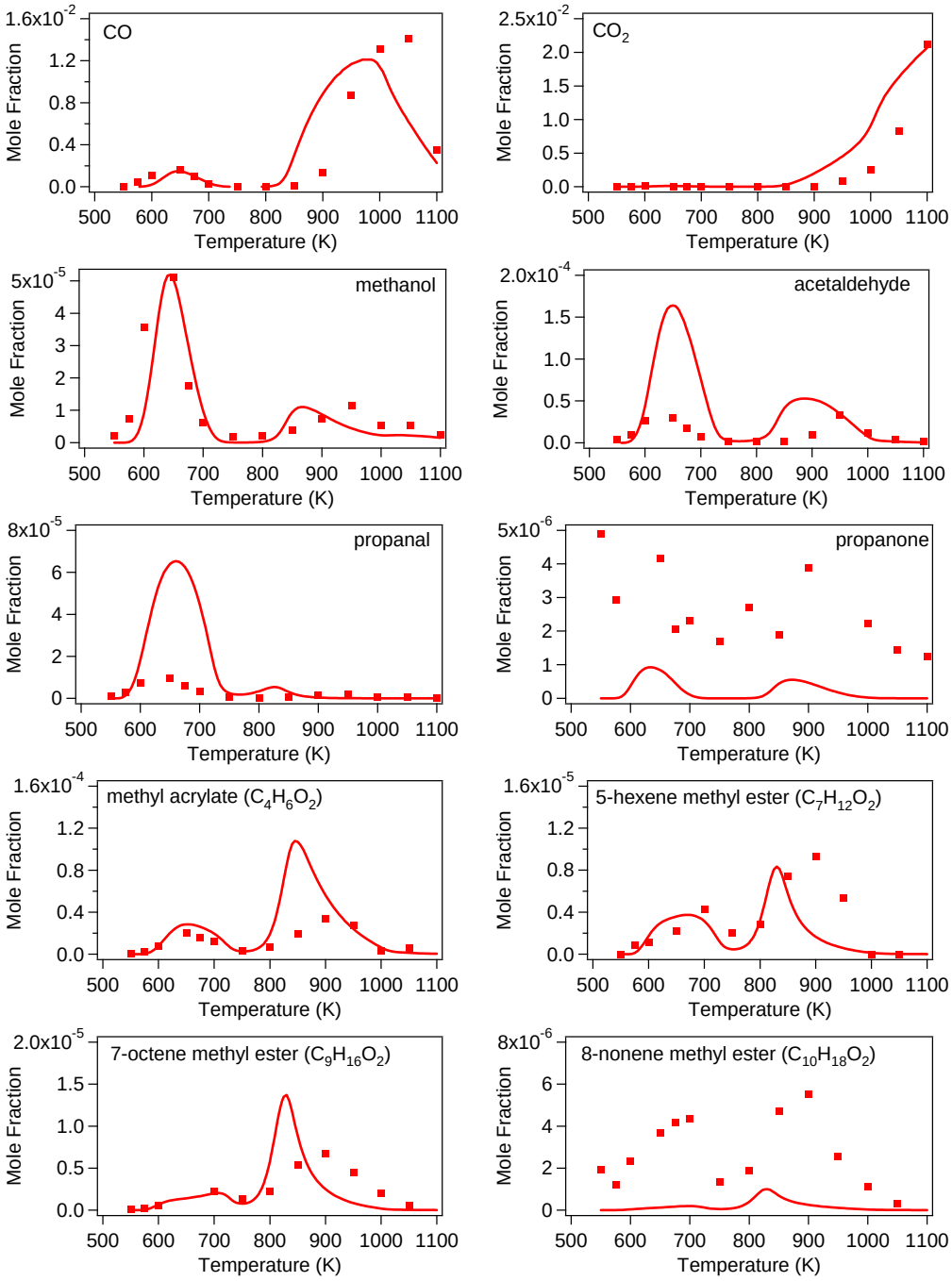

Figure 12: Comparison of the n-heptane/methyl decanoate model (——) with n-decane/methyl palmitate jet-stirred experiments (▪) [38]. Mole fraction profiles of oxygenated compounds.

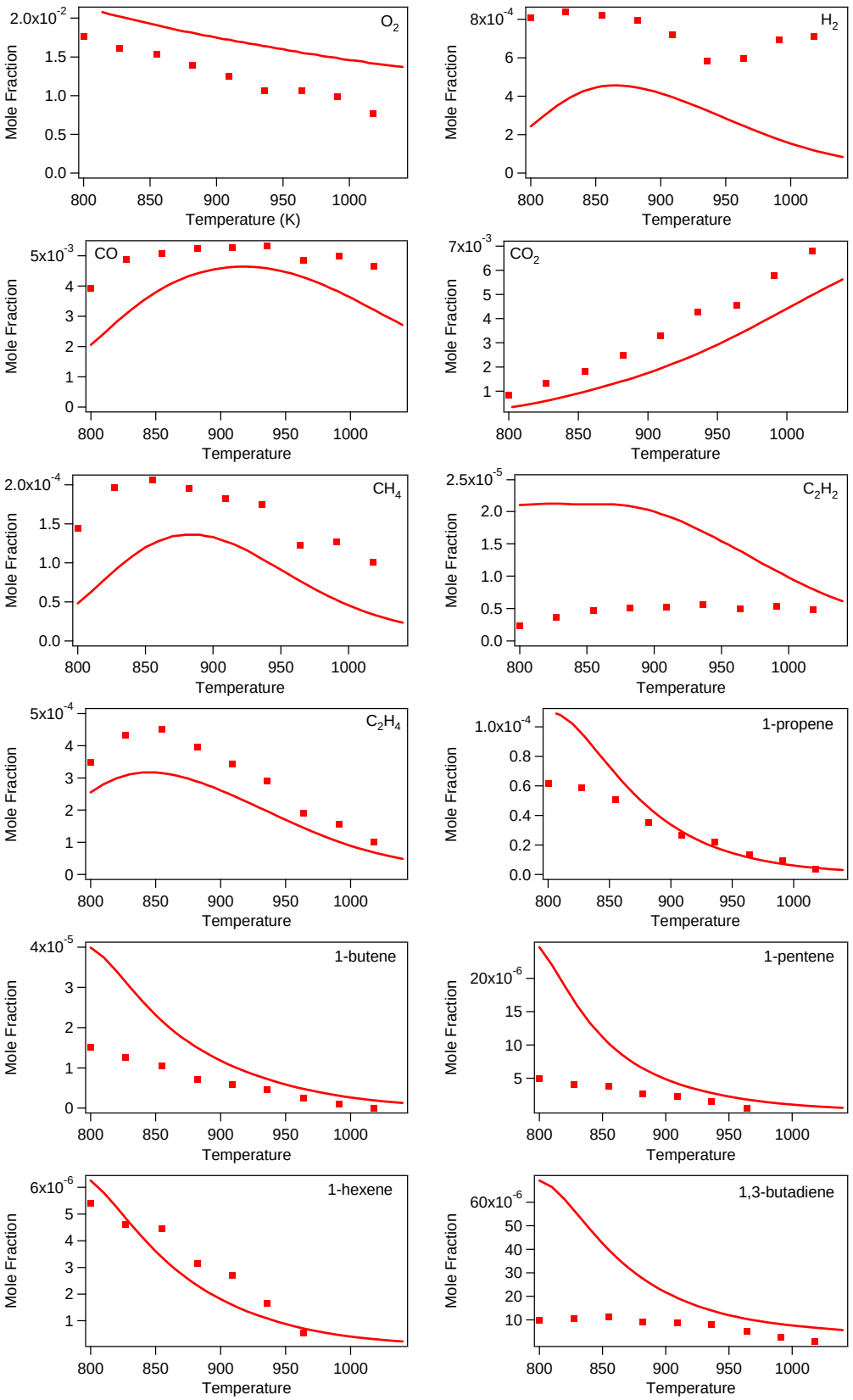

Figure13: Comparison of the n-heptane/methyl decanoate/methyl-9-decenoate model (——) with rapeseed oil methyl esters jet-stirred experiments (▪) [16].

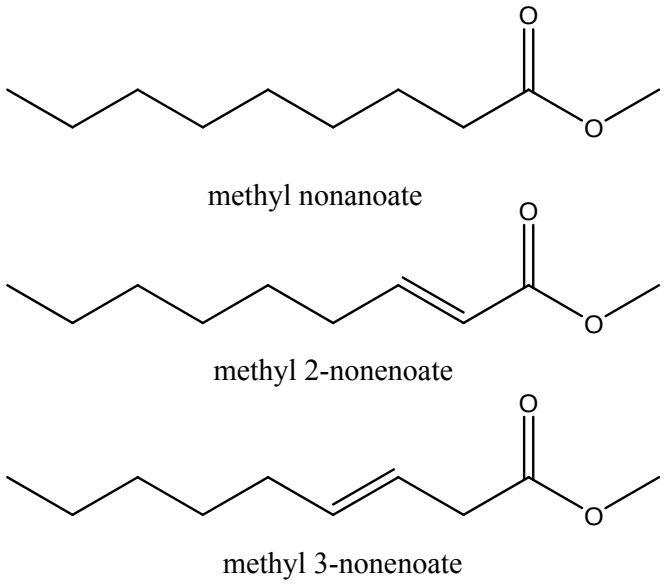

Figure 14: Structures of C_9 methyl esters investigated in a motored engine study [18].

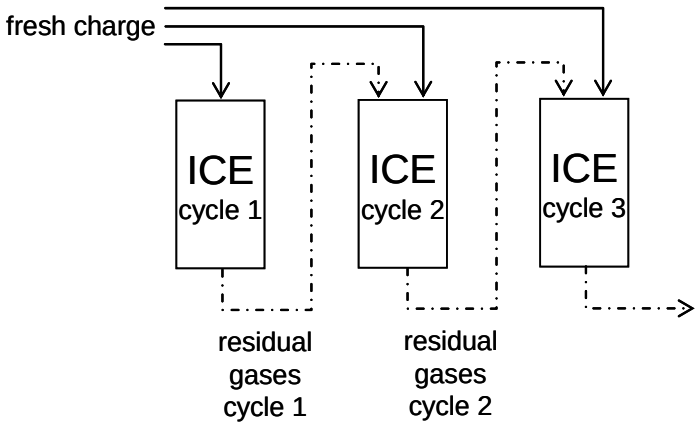

Figure 15: Gases in the residual part of the cylinder were taking in account by considering consecutive cycles. (ICE=internal combustion engine)

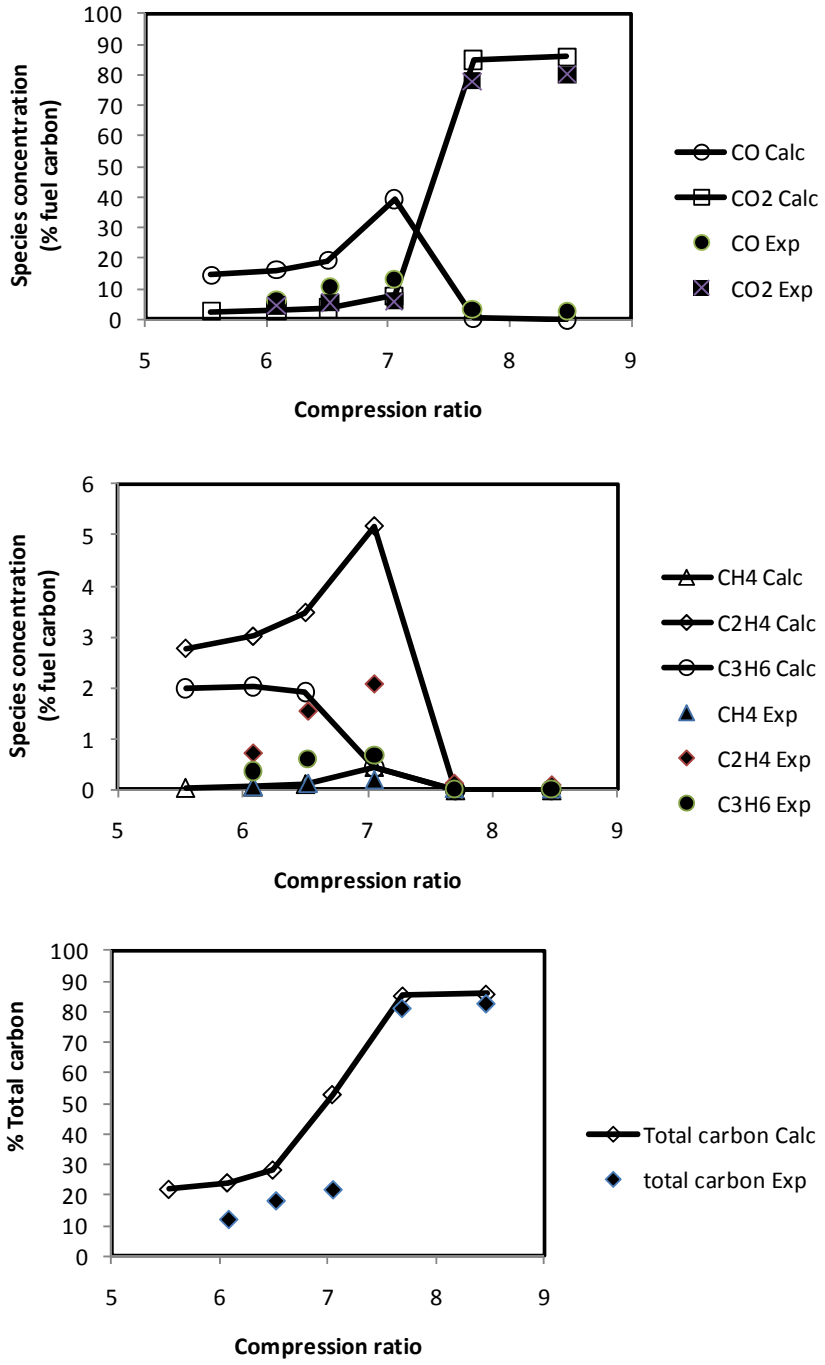

Figure 16: Comparison of predicted and measured [18] species exhausted from the motored engine. (Fuel: methyl-5-decenoate (model), methyl-2-nonenoate (experiments). Equivalence ratio of 0.25 and 600 rev/min.